Targeted diagnostic magnetic nanoparticles for medical imaging of pancreatic cancer

I. Rosenberger [a,e,1], A. Strauss [b,1], S. Dobiasch [d], C. Weis [b], S. Szanyi [d], L. Gil-Iceta [c], E. Alonso [c],

M. González Esparza [c], V. Gómez-Vallejo [c], B. Szczupak [c], S. Plaza-García [c], S. Mirzaei [e], L.L. Israel [f], S.

Bianchessi [g], E. Scanziani [g], J.-P. Lellouche [f], P. Knoll [e], J. Werner [d,h], K. Felix [d], L. Grenacher [b], T. Reese [c],

J. Kreuter [a,*], M. Jiménez-González [c]

[a] *Institute of Pharmaceutical Technology, Biocenter Niederursel, Goethe University, Max-von-Laue-Str. 9, 60438 Frankfurt/Main, Germany*

[b] *Department of Diagnostic Radiology, University of Heidelberg, Im Neuenheimer Feld 110, 69120 Heidelberg, Germany*

[c] *CIC biomaGUNE, Molecular Imaging Unit, Paseo Miramón No 182, Parque Tecnológico de San Sebastián, 20009 San Sebastián, Guipúzcoa, Spain*

[d] *Department of General and Visceral Surgery, University of Heidelberg, Im Neuenheimer Feld 110, 69120 Heidelberg, Germany*

[e] *Wilhelimnenspital, Institute of Nuclear Medicine, Montleartstr. 37, 1160 Wien, Austria*

[f] *Department of Chemistry & Institute of Nanotechnology & Advanced Materials, Bar-Ilan University, Ramat-Gan 5290002, Israel*

[g] *Fondazione Filarete, Viale Ortles 22/4, 20139 Milano, Italy*

[h] *Department of General-, Visceral-, Transplantation-, Vascular- and Thorax-Surgery LMU Munich, Marchioninistr. 15, 81377 Munich, Germany*

Abstract

Highly aggressive cancer types such as pancreatic cancer possess a mortality rate of up to 80% within the first 6months after diagnosis. To reduce this high mortality rate, more sensitive diagnostic tools allowing an early stagemedical imaging of even very small tumours are needed. For this purpose, magnetic, biodegradable nanoparticles prepared using recombinant human serum albumin (rHSA) and incorporated iron oxide (maghemite, γ-Fe$_2$O$_3$)nanoparticles were developed. Galectin-1 has been chosen as target receptor as this protein is upregulated in pancreatic cancer and its precursor lesions but not in healthy pancreatic tissue nor in pancreatitis. Tissue plasmin-ogen activator derived peptides (t-PA-ligands), that have a high affinity to galectin-1 have been chosen as target moieties and were covalently attached onto the nanoparticle surface. Improved targeting and imaging propertieswere shown in mice using single photon emission computed tomography–computer tomography (SPECT–CT), a handheld gamma camera, and magnetic resonance imaging (MRI).

1. Introduction

During the last decades the development of early diagnostic methods for various tumours enabled an improvement in the treatment of cancer patients. This achievement, however, has not been achieved for pancreatic ductal adenocarcinoma (PDAC). PDAC is currently the fourth leading cause of cancer death in the United States of America [1]. Furthermore it is anticipated to become the second leading cause of cancerrelated deaths in the year 2030 [1,2]. PDAC possesses a mortality rate of up to 80% within the first 6 months after diagnosis [3], and the 5-year survival rate is only 6.7% [4,5].

The paramount problem with pancreatic adenocarcinoma is that in most cases this cancer is diagnosed only in late stages, after possible metastasis spread, especially into the liver. Only 10%–15% of patients are diagnosed in the early stages of the disease [6].

Magnetic resonance imaging (MRI), computed tomography (CT),and single photon emission computed tomography–computer tomography (SPECT–CT) are state of the art in the diagnosis of pancreatic tumours. However, these medical imaging methods often don't have theability to distinguish pancreatitis from pancreatic cancer [7], which iseven worse as pancreatitis is a risk factor for carcinogenesis. Even the addition of more sophisticated imaging techniques such as diffusionweighted imaging is of no help in this effort [8].

In preclinical MRI studies, such as s of tumour cell migration and regional tumour growth, contrast enhanced MRI is used for both, diagnostic purposes and therapeutic monitoring. (Super-)paramagnetic nanoparticles offer the advantage, that they can be visualized in the morphologicstandard T1-weighted (T1w) and T2-weighted (T2w) sequences.

NPs represent a novel class of therapeutics and diagnostics for cancertherapy. Recent studies demonstrated that therapeutics bound to or encapsulated into NPs provide an enhanced efficacy as well as reducedside effects compared to the respective unbound therapeutic entities[9–11]. Due to the leaky vasculature within a variety of tumours combined with their poor lymphatic drainage, nanoparticles can selectivelyaccumulate in the tumour tissue following intravenous injection [12]. Inaddition, the attachment of targeting ligands that can bind to receptorsor other biochemical structures which are presented and overexpressedon the surface of cancer cells, enhances the interaction with these cellsresulting in further increase of accumulation in the tumour. Moreover, the targeting ligands also promote internalization by receptormediated endocytosis [13,14], which is a prerequisite for advanced in tracellular therapeutic approaches such as interference with the cells' metabolism via siRNA. Tumour-associated antigens that are already atearlier stages highly expressed on the cell surface of cancer cells butnot in neighbouring tissue or only in negligible amounts are ideal for tumour targeting. Attachment or incorporation of diagnostic markers thuscould allow the detection of the tumour by the targeted NPs using medical imaging. Since pancreatic adenocarcinomas are tumours witha very low perfusion (hypovascularized tumours) and hence radiologically low contrast agent uptake, a nanoparticle accumulation in these tumours, therefore, would be of great help for diagnosis as well as therapy.

Previous studies showed that these magnetic NPs (MNPs) consisting
of recombinant human serum albumin (rHSA) and a magnetic core are non-toxic in vitro and in vivo and exhibited promising in vitroMRI-behaviour [15]. The main advantage of MNPs is their ability tocovalently bind different molecules to their surface for presentation tocellular molecular units such as receptors. Loaded NPs were able to release the drug or diagnostic agent after internalization and procession of the particles in the targeted tissue, by using different binding techniques as described by Wartlick et al. and Weber et al. [11,16]. Thisfact underlines the versatility of these particles in the scope of modularnanosystem platforms.

Recently, it was shown that the galectin-family (Gal), especially galectin-1 (Gal-1), acts as functional receptors for tissue plasminogenactivator (t-PA) [17]. The binding is specific with a strong affinity and,hence, may provide a promising strategy for pancreatic cancer targeting.The expression of Gal-1 was reported to be upregulated in pancreaticcancer cells but is not expressed

69   in adjacent normal tissues or adjacent inflammatory pancreas [18,19].

70   The prime objective of the present study is to investigate different

71   in vivo imaging procedures for their ability to improve the pancreaticcancer diagnosis using non-toxic human serum albumin

72   nanoparticlesthat offer the possibility for attachment of a variety of targeting ligandsand, as a further step, allow the binding of

73   drugs (theranostics). As targeting moiety glycosylated peptides derived from t-PA, Gal-1's natural ligand, were bound

74   covalently to previously developed [15] magnetic maghemite-containing nanoparticles (MNPs). The targeted MNPs were

75   physico-chemically characterized, and their potentialin vivo toxicity was determined by histology. The in vivo imaging

76   methods included MRI as well as SPECT-CT and handheld gamma camera after radiolabelling the MNPs with ^{67}Ga.

77   2.   Materials and methods

78   *2.1.   Nanoparticle preparation*

79   MNPs were prepared following a method previously described byRosenberger et al. [15]. For the incorporation of the magnetic

80   γ-CANmaghemite NPs (CAN, $(NH_4)_2Ce(IV)(NO_3)_6$-γ-Fe_2O_3 NPs) into the rHSA nanoparticles, rHSA (Sigma-Aldrich, Steinheim,

81   Germany) was dissolved to 100 mg/mL in 10 mM NaCl solution. 2000 μg or 4000 μgiron, respectively, were added to the protein

82   solution and incubated for1 h at 20 °C (Eppendorf thermomixer, 300 rpm, Hamburg, Germany). Af-terwards desolvation took place

83   by addition of 4 mL ethanol 96% (V/V)under constant stirring with a pump rate of 1 mL/min (ISMATEC IPN, Glattbrugg,

84   Switzerland). This procedure allowed a defined nanoparticleformation process. By using 117.5 μL glutaraldehyde 8% (v/v) (Sigma-

85   Aldrich, Steinheim, Germany) as a bifunctional crosslinker, the freeavailable amino groups on the surface of the denaturized

86   protein wereinactivated. The amount of required glutaraldehyde was calculated on the basis of 60 amino groups per molecule of

87   rHSA. This bifunctionalaldehyde was then added in excess in a quantity that would be required to crosslink 200% of these groups.

88   The nanoparticle suspension wasstirred at room temperature over 24 h to ensure the crosslinking process to be quantitative.

89   To remove free glutaraldehyde, denaturized protein, and γ-CAN maghemite NPs in excess, three cycles of centrifugation (20

90   min, × 20,100 rcf) and resuspension of the centrifugation pellet in 1 mL ultra-purified water is necessary. Each resuspension step

91   was performed inan ultrasonic bath (Bandelin, Sonorex, Berlin, Germany). Finally, theamount of MNPs in suspension was

92   determined gravimetrically.

93   The particle size, size distribution (PDI), and surface charge (ZP) of the obtained MNPs were determined by dynamic light

94   scattering (DLS) using a Zetasizer Malvern Nano ZS (Malvern Instruments Ltd., Malvern, UK). For this purpose, a 10 μL MNP

95   suspension was diluted with ultrapure water to 1 mL 1,4,7,10-tetraazacyclododecane-1,4,7,10-tetraacetic-NHS (DOTA- NHS) ester

96   (CheMatech, Dijon, France) as chelator for ^{67}Ga was attachedonto the surface of the MNPs using 1-ethyl-3-(3-dimethylamino-

97   propyl)carbodiimide (EDC) as crosslinking moiety. Briefly, 5 mg MNP was resuspended in 0.1 M 2-(N-morpholino) ethanesulfonic

98   acid buffer(MES buffer) (Thermo Fisher Scientific Inc., Rockford, USA) and incubated with a 10-fold molar excess of EDC and 5 mg

99   DOTA-NHS for 1 h at roomtemperature. Afterwards, the DOTA-MNPs were purified three times bycentrifugation and resuspension

100   in Milli-Q water as described above.The amount of unbound DOTA-NHS ester in the supernatant was determined using HPLC

101   analysis.

102 As targeting moiety tPApep.1$_{LAC}$ was selected (see SI, *t-PA peptidesand galectins interaction studies*, SI Table S1). This sequence was

103 synthetized by Peptide Specialty Laboratories GmbH, Heidelberg, Germany. 50 µg tPApep.1$_{LAC}$ (Peptide Specialty Laboratories

104 GmbH, Heidelberg, Germany) was attached onto the surface of DOTA-MNPs using the same binding protocol as described

105 above. The amount of unbound protein in the supernatant was determined using a FLUOstar Galaxy (MTXLab Systems, Inc.,

106 Virginia, U.S.A.). The attached number of tPApep.1$_{LAC}$per nanoparticle was calculated using a modified equation by Nobs et al.[20]:

107 $$n = a \cdot N \cdot \frac{4}{3}\pi r^3 \cdot d$$

108 Equation 1: n = number of targeting moieties per MNP, a = mol of targeting moiety per MNP [g], N = Avogadro number (6.022

109 $\times 10^{23}$), r = mean radius of MNPs, d = density of MNPs [g/cm^3] (set as 1 g/cm^3).

110 The obtained DOTA-MNPs incubated with 2000 µg iron were used for MRI 11.7 T experiments, SPECT–CT and handheld gamma

111 camera scans, whereas MNPs incubated with 4000 µg of iron were employedfor MRI investigations at 1.5 T.

2.2.   Cell culture

113 The human pancreatic tumour cell line PANC-1 was obtained from the European Collection of Cell Cultures (ECACC Cell Lines,

114 Sigma Aldrich). PANC-1 cells were maintained as monolayer culture in RPMI-1640 (Lonza, Verviers, Belgium) with 10% FCS

115 (Sigma-Aldrich, St. Louis USA), 1% streptomycin/penicillin (Invitrogen, USA) and 2 mM glutamine (Lonza,, Verviers, Belgium).

116 Cultures were grown at 37 °C in ahumidified atmosphere of 5% CO_2/95% air. Regular testing of the presence of Mycoplasma was

117 performed with the use of a commercialkit (Lonza, Rockland, ME, USA).

2.3. Magnetic resonance at 11.7 T, SPECT/CT and handheld gamma camerain vivo imaging experiments using DOTA-2000-MNPs

119 All experiments described within this section, and only those, wereperformed in the molecular imaging facility in San Sebastián

120 (Spain). Experimental design, execution, data acquisition, and analysis as well as interpretation were performed by

121 CICbiomagune staff. Handheldgamma camera experiments were performed and interpreted by researchers from Vienna

122 (Austria).

2.3.1. Tumour Xenograft

124 All animal procedures utilizing SPECT/CT, 11.7 T MRI and the hand-held gamma camera were performed in accordance with the

125 Spanishpolicy for animal protection (RD53/2013), which meets the requirements of the European Union directive 2010/63/UE

126 regarding the protection of animals used in experimental procedures. The guidelines were approved by the Ethical Committee

127 of CIC biomaGUNE and authorized by the regional government.

128 Preparation of PANC-1 cells for production of xenografts consisted ofcollecting them in a pellet by centrifugation and a further

129 suspension inDulbecco's Phosphate Buffered Saline (PBS) (Lonza, Verviers, Belgium)at a concentration of 20×10^6 cells/mL. The

130 cell suspension was mixed with Matrigel (Becton Dickinson, Oak Park, Bedford, MA) kept at 4 °C at a 1:1 (v/v) ratio, and finally

131 200 µL of the mixture was usedfor each injection. Fourteen seven-week old male athymic-nude CD-1Foxn1 nu/nu mice (Charles

132 River Laboratories, Calco, Italy) were injected subcutaneously with 2 million PANC-1 cells in the upper leftflank. Mice were

133 housed in a controlled environment (12 h:12 h light/dark cycle with dawn and dusk transitional periods, room temperature 22 °C

134 and 55% relative humidity) and maintained on an ad libitum access to commercially available pelleted diet (Teklad 2919,

135 Harlan Laboratories, Inc.) and sterilized water. Animal weight and tumoursize were monitored three times per week. The

136 tumour volume was calculated using the formula $(L \times W^2)/2$ where L is the longest diameter (inmm) of the tumour and W (in mm)

137 is the longest perpendicular diameter with respect to L. Both dimensions were determined with acalliper (see SI, Figure S1).

138 When tumour volumes reached above 150 mm^3 (approximately after 8/10 weeks post-inoculation of the cells), animals were

139 subjected to the imaging sessions.

140 *2.3.2. MRI at 11.7 T*

141 MRI measurements were performed on an 11.7 T horizontal boreBiospec 117/16 scanner (Bruker, Ettlingen, Germany) using

142 a 40 mmtransmit/receive volumetric coil. Mice were anaesthetized using 4.5%– 5% isoflurane and maintained during images

143 acquisitions at 1.5%–2.5% in O_2. Animals were prevented from hypothermia with the use of a water blanket, and respiration

144 was monitored. Baseline scans were performed prior to the injection of MNPs (i.v.), and imaging continued up to 2 h. An

145 additional imaging session was conducted the following day. Axial images were acquired to cover continuously the tumour

146 (12 mm-15.6 mm), using a slice thickness of 0.6 mm. The field of view (FOV) was 30×30 mm^2 resulting in an inplane resolution

147 of 234×234 µm^2. A respiration triggered gradient echo sequence (TE = 3.1 ms) was selected for T1w imaging, whereas a triggered

148 RARE (Rapid Acquisition with Relaxation Enhancement) sequence (TEef f = 13.40 ms, RAREfactor = 4) was chosen for T2w imaging.

149 Both, DOTA-2000-MNPsand DOTA-tPApep.1$_{LAC}$-2000-MNP (1.4 mg Fe/kg each) were tested (n = 2).

150 *2.3.3 Radiolabelling*

151 The gamma-emitting ^{67}Ga radionuclide ($t_{1/2}$ = 3.26 days) was purchased from Molypharma S.L. as a citrate solution; this

152 radioisotope wasselected because of its long half-life, which enabled the longitudinalfollow-up of the biodistribution pattern up

153 to several days. The citratesolution was passed through a C18 Sep-Pak silica plus light cartridge (Waters chromatography, S.A.),

154 which was then washed with ultrapurewater. Desorption of gallium was performed by addition of 1 mL 0.1 MHCl 30% (v/v) solution

155 (Merck kGaA, Darmstadt, Germany). The eluatewas collected in 10 different fractions, and only those containing themaximum

156 activity concentration were used in subsequent labelling experiments. The labelling procedure can be summarized as follows: The

157 radioactivity contained in one of the fractions was mixed with 200 µLof a buffered sodium acetate solution obtained from Sigma-

158 Aldrich Co. LLC (0.2 M, pH = 3.8) together with 50 µL of the DOTA-2000-MNP orDOTA-tPApep.1$_{LAC}$-2000-MNP solution (10

159 mg/mL). The pH was adjusted to 3.8 approximately by titration with 1 M NaOH, and the reactionwas allowed to occur at 55 °C,

160 using a digital block heater (SBH130D,Stuart Group Ltd.) for 30 min. Thereafter, the crude material was purified via centrifugal

161 filtration (8 min, 8000 rpm) through Millipore filters (100 kDa cut-off). The resulting precipitate was washed three timeswith

162 sodium acetate buffered solution, and the radiochemical yield was calculated as the ratio between the amount of radioactivity

163 in thefilter and the starting radioactivity.

164 *2.3.3. Radiochemical integrity*

165 A good approximation for the determination of the radiochemicalintegrity of NPs in vivo consists of assessing the integrity in

166 vitro by incubating the NPs in a fluid that mimics in vivo conditions, e.g. a solution containing a strong chelator [21,22]. In our

167 experiments, DOTA-2000- MNPs and DOTA-tPApep.1$_{LAC}$-2000-MNP were prepared and purified as described above, and the

168 radiochemical integrity was determined in two different media. Briefly, MNPs were resuspended in 400 μL of physiologic NaCl 0.9%

169 solution (Braun Medical S.A.). The suspension was then divided into 8 different aliquots containing 50 μL of the MNPs each,

170 which were treated as follows: 4 samples were mixed with a solution of the bifunctional chelator DOTA (Macrocyclics Inc. Dallas,

171 USA, final concentration = 32 μM); 4 samples were diluted with an equal volume of physiologic saline solution. The aliquots

172 were incubated at 37 °C for 1, 3, 24 and 48 h, respectively. The samples were then filtered in order to separate the NPs from the

173 media, and the radioactivity was measured in a 2470 WIZARD^2 Automatic Gamma Counter (PerkinElmer). The dissociation

174 of ^{67}Ga (expressed in percentage) from the radiolabeled nanoparticles at each time point was calculated as the ratio between the

175 amount of radioactivity in the filter and the starting amount of radioactivity.

176 *2.3.4. SPECT–CT*

177 Three hours before the examination, PANC-1 mice (Charles River, Calco, Italy) bearing the subcutaneous tumour received an

178 intravenous administration of the radiolabelled nanoparticles (6.5 ± 0.4 MBq for DOTA-2000-MNP, 6.6 ± 1.3 MBq for DOTA-

179 tPApep.1$_{LAC}$-2000-MNP,

180 V = 150-200 μL in physiologic saline solution). During image acquisi-tion, anaesthesia of the animals at first was induced

181 using 4.5%–5% isoflurane (IsoFlo®, Abbott Laboratories) and maintained with 1.5%– 2% isoflurane in O$_2$. Images were acquired

182 using a eXplore speCZT CT preclinical imaging system (GE Healthcare, USA) placing the animals on top of a homeothermic blanket

183 control unit (Bruker BioSpin GmbH, Karlsruhe, Germany) to prevent hypothermia. Once the animals were positioned within the

184 field of view of the system, whole-body SPECT– CT scans were acquired at 3 h, 24 h, and 48 h post-injection for 30 min, 60

185 min, or 120 min. As a general rule, the image acquisition period was dependent on the counts detected by the collimator of the

186 scanner, thus, longer imaging times were needed as the gamma emissions decreased. After each SPECT scan, CT acquisitions were

187 performed to provide anatomical information of each animal. The SPECT images were reconstructed using an ordered-subset

188 expectation maximization (OSEM) iterative algorithm (3 iterations/5 subsets, 128 × 128 × 32 array with a voxel size of 0.4 ×

189 0.4 × 2.46 mm^3), whereas for the CT a cone beam filtered back-projection a Feldkamp algorithm (437 × 437 × 523 array with

190 a voxel size of 0.2 × 0.2 × 0.2 mm^3) was used.

191 After SPECT–CT images reconstruction, image data was quantified by PMOD analysis software (version 3.4, PMOD Technologies Ltd.).

192 SPECT images were co-registered with CT images; the volumes of interest (VOIs) were drawn around the organs under

193 investigation (tumour and muscle), and results of the SPECT signal were used to calculate the tumour-to-muscle ratio.

194 Differences between groups were analysed using an unpaired two-tailed *t*-test, whereas temporal evolution within groups was

195 assessed by a paired two-tailed *t*-test. In both cases, we considered a threshold for statistical significance at p ɓ 0.05.

196 *2.3.5.   Handheld gamma camera*

197 The handheld gamma camera (CrystalCam, Crystal Photonics GmbH, Berlin, Germany) (see also SI *Handheld gamma camera*) also can

198 be used for preclinical imaging with a special positioning adapter. In the present study, the 7-week-old athymic-nude CD-1 Foxn1

199 nu/nu mice (CharlesRiver, Calco, Italy) were put on top of the imaging device. The sides ofthe camera were shielded with 3 mm

200 lead. This device can be used forenergies from 50 keV till 250 keV. The handheld gamma camera wasplugged into a standard

201 laptop via an USB-interface. With installedvisualization software, collected events were continuously transmitted to the laptop

202 via the USB port [23].

203 *2.4. R2 Magnetic resonance in vivo imaging experiments using 4000-MNPsat 1.5 T*

204 All experiments described within this section, and only those, wereperformed in the Department of Diagnostic Radiology in

205 Heidelberg(Germany). Experimental design, execution, data acquisition and analysis as well as interpretation were performed

206 by staff members ofthe University of Heidelberg.

207 *2.4.1. Tumour mouse models*

208 All experiments on animals were officially approved by the EthicalCommittee of the University of Heidelberg and Regional

209 Commission Karlsruhe, Germany (ref. no. 35-9185.81/G-9/12) in accordance withthe German law for the care and use of

210 laboratory animals.

211 Human pancreatic carcinoma cell line PANC-1 was obtained fromAmerican Type Culture Collection (Manassas, VA, USA). Cells

212 were cultured in RPMI-1640 medium supplemented with 10% fetal bovine serum (FBS), 100 U/mL penicillin, and 100 μg/mL

213 streptomycin (Invitrogen GmbH, Karlsruhe, Germany) at 37 °C in a humidified 5% CO_2 atmosphere.

214 For the subcutaneous tumour model ~ 2×10^6 PANC-cells resus- pended in 50 μL RPMI-1640 were injected subcutaneously into the

215 anterior region of the mouse trunk of female 5-6-week old CD nuBR mice(crl:CD1-Foxn1^{nu}) (Charles River Laboratories,

216 Sulzfeld, Germany) through a 26-gauge needle. The injection sites were examined daily.Ten days post-injection the appearing

217 tumours were measured twiceweekly with Vernier calliper and tumour volumes were calculated asdescribed above. The sc

218 tumours were allowed to grow for about4 weeks to 5 weeks until approximately 0.5 cm^3 in size and then subjected to NP

219 treatment and MRI investigations. When experiments were finished, animals were sacrificed and tumours and organ of inter-

220 est were excised, spitted part flash frozen in liquid nitrogen and storedat −80 °C other part fixed, and embedded in paraffin wax

221 for furtheranalysis.

222 For the orthotopic (ot) tumour model the tumour cell inoculationwas performed by direct injection in the pancreatic tail via

223 laparotomy.In this case 6-week old female CD nuBR mice (Charles River Laborato-ries) were first anaesthetized with 3%

224 isoflurane (Isofluran Baxter, Baxter Deutschland GmbH, Unterschleissheim, Germany), fixed on a surgical board and

225 maintained with 1.5%–2% isoflurane mixed with O_2 600 mmHg. A left lateral abdominal incision of approximately 1 cm-1.5 cm

226 was made, the peritoneum was opened the spleen with tail ofthe pancreas was exteriorized with cotton swabs, and using an

227 Insulin syringe 27G × 1.2 in 1.0 mL (Terumo, Eschborn, Germany) ~ 2×10^6 Panc-1 cells in 20 μL PBS were gently injected into the

228 pancreatic parenchyma. The exteriorized organs were placed back into the abdominalcavity; the peritoneum and the skin were

229 then closed with 5-0 surgicalsuture (Johnson & Johnson Medical GmbH, Ethicon Deutschland, Norderstedt, Germany). The

230 wound healing, body weight and physical condition of the animals was monitored over the total experimental time. Tumour

231 growth was assessed by palpation and by high- frequency ultrasound imaging, with a Vevo 770® High-Resolution Imaging

232   System, (Visual Sonics, Amsterdam, Netherlands).

233   *2.4.2.*   *R2 MRI*

234   In addition to the MRI measurements with a 11.7 T instrument, experiments where performed using a 1.5 T generally available

235   humanwhole-body MR-scanner (Siemens Magnetom Symphony, Erlangen, Germany) with a custommade radiofrequency coil

236   (animal resonator)(SI Figure S2) for signal reception. This pickup-coil was designed as acylindrical volume resonator with an

237   inner diameter of 35 mm and ausable length of 100 mm.

238   For MRI examination and catheterization, female mice CD-1 (nu/nu)(Charles River Laboratories, Research Models and Services,

239   Sulzfeld, Germany) were anaesthetized by inhalation of a mixture of isofluorane (1.5%), and O_2, flow was adjusted to the individual

240   need of the animal.The tail vein was catheterized using a 30 G needle connected to a

241   10 cm PE 10 polyethylene catheter (Portex, Medic Eschmann, Germany) filled with 0.9% NaCl. Successful puncture of the

242   tail veinwas controlled by blood reflux into the catheter and by injectionof 30 μL 0.9% NaCl. 100 μL of 4000-MNP and

243   tPApep.1$_{LAC}$-4000-MNP (10 mg/mL), respectively, were injected as bolus within 5 s into the tail vein of the nude mice manually.

244   The injected amount of iron in term of γ-CAN maghemite was about 20 μg per injection.

245   All animals were examined with multiple axial high-resolution T2wturbo spin echo (TSE) pulse sequences, using the following

246   imaging parameters: TR = 4390 ms, TE = [12 ms, 24 ms, 60 ms], TA = 7:38,

247   NA = 5, field of view = $40 \times 54 \times 55$ mm^2, matrix = $144 \times 192 \times 46$,slice thickness = 1.20 mm, voxel size = $0.28 \times 0.28 \times 1.20$

248   mm^3. During an overall measurement time of ~105 min, 13 measurements were obtained (SI Table S2). Slices were placed to cover

249   the mice's liver, kidneys,muscle (the norm), the sc tumour, and the ot tumour. The tissue typeswere analysed in terms of the

250   temporal behaviour of the signal intensityand, furthermore, the spin–spin–relaxation rate was calculated before and 90 min after

251   MNP administration according to Weis et al. [24]. This method has been chosen to simulate the most common clinical settingof

252   MRI systems.

253   3.   Results

254   *3.1.   Physico-chemical characterization of the nanoparticles*

255   In a first step, magnetic nanoparticles (MNPs) were prepared using rHSA as shell protein and CAN-maghemite NPs as contrast

256   agent for MRI. To ensure that the iron is encapsulated into the rHSA NP matrix,transmission electron microscopy pictures were

257   taken previously. In these pictures, CAN-maghemite is visible in form of black spots surrounded by the grey rHSA

258   nanoparticle matrix in transmission electron microscopy images [15]. The MNPs were characterized by PCS to obtain particle

259   diameter, PDI and ZP (Figures S3 and S4). All pa-rameters were also determined after the attachment of DOTA as a che-lator for

260   radio-imaging and t-PApep.1$_{LAC}$ as the targeting moiety (DOTA-t-PApep.1$_{LAC}$-2000-MNP and t-PApep.1$_{LAC}$-4000-MNP,

261   respectively).

262   Covalent linkage of the DOTA chelator was achieved in an amount of49% ± 1.2%. The amount of covalently bound t-PApep.1$_{LAC}$ to

263   DOTA-2000-MNP and 4000-MNP, respectively, is shown in Table 1.

264   All targeted nanoparticles were also investigated regarding the number of attached targeting moieties per MNP. The number

265 of t-PApep.1$_{LAC}$ covalently linked to the surface of DOTA-2000-MNP 4000-MNP, respectively, was calculated using Equation 1

266 (Table 1):

267 As shown in SI Figures S3 and S4, all nanoparticles were comparable in size. A small shift in size distribution could be observed, and

268 the surface charge changed from a negative charge in case of "naked" MNPs to a positive charge in case of targeted MNPs. The resulting

269 targeted MNPs containing different amounts of iron in term of CAN-maghemite show similar particle sizes and particle size

270 distributions and in vivo toxicities[15].

3.2. MRI (11.7 T)

272 In T1w images, the tumour tissue appears generally homogeneous, with dark areas of low signal intensity, whereas the T2w images

273 show larger tumour heterogeneity. Following the administration of MNPs, neither T1w nor T2w images indicate a fast and strong MNP

274 accumulation within the first 2 h (Fig. 1). However, the following day the tumours appeared more heterogeneous in signal intensity,

275 indicating a slow MNP uptake. Larger bright regions were diffuse and might reflect very low concentrations due to a

276 predominant T1 effect whereas focal dark spots could indicate high concentrations due to T2 shortening (Fig. 2). No difference

277 between DOTA-2000-MNPs and DOTA-tPApep.1$_{LAC}$- 2000-MNP was found.

3.3. R2 MRI (1.5 T)

279 Signal intensities (SIs) were normalized to the region of interest's (ROIs) values before MNP injection. ROIs were analysed in

280 images before MNP administration and 90 min afterwards (decreased SIs representing increased uptake).

281 For the non-targeted MNPs, only the liver showed a significant signal intensity drop caused by the NPs' presence. Both tumour species,

282 kidneys, and the muscle had the same signal intensities before and after NP administration. The targeted MNPs showed a loss in

283 signal intensity for all ROIs (both tumour species, liver, and kidneys), except the ROI containing the background (muscle). The

284 signal drop for each ROI, however, was not statistically significant (SI, Table S3).

285 In addition to conventional SI quantification, the R2 relaxation rates were measured before MNP administration and 90 min

286 afterwards (see SI Table S4). The sc tumour and the kidneys expressed a slightly increased but not significantly different

287 relaxation rate before and after MNP administration (Fig. 3, top). The liver showed a significant R2-increase due to the non-

288 targeted MNP influence on the spin–spin– relaxation. The orthotopic (ot) tumour and muscle changes in R2 were within the

289 range of the standard deviations and not significant. These results are in agreement with the SIs measured for the mice with an

290 injection of non-targeted NPs (Fig. 3, A1, A2, C1, and C2).

291 The administration of targeted MNPs led to a significant R2-increase in the sc tumour (Fig. 3, B1, B2, D1, and D2). The ot tumour and

292 the liver also had an increase in spin–spin–relaxation rate, but not as strong as the sc tumour (see SI Table S4). The kidneys and

293 the muscle, however, expressed a comparable R2 before and after injection of targeted NP. Consequently, the further focus was

294 on the sc tumour for detailed discussion and visualization.

295 Comparing normalized R2 of the sc tumour before and after NPs administration revealed in both cases that the relaxation rate

296 increased (Table 2). In terms of the non-targeted NP, R2 was increased by a factor of 1.92. In terms of the targeted NPs, R2 increased

297 by a factor of 2.69 indicating increased uptake by addition of the target moiety.

3.4. Radiolabelling and radiochemical integrity of DOTA-2000-MNPs and DOTA-t-PApep.1$_{LAC}$-2000-MNP

The radiochemical yield was calculated as the ratio between the amount of radioactivity in the filter (after 3 consecutive washings) and the starting amount of radioactivity. Radiochemical yield valueswere 56% ± 15% and 62% ± 23% for DOTA-2000-MNPs and DOTA-t-PApep.1$_{LAC}$-2000-MNP, respectively.

The in vitro stability of radiolabelled DOTA-2000-MNP and DOTA-t-PApep.1$_{LAC}$-2000-MNP was studied by incubating the MNPs both inphysiologic saline solution and in the presence of the competing chelator DOTA at 37 °C (incubation time: 1 h-48 h), submitting to centrifugalfiltration, and measuring the amount of radioactivity in the filtrate andin the filter using a gamma counter. Both NPs showed excellent stabilityin physiologic saline solution, with 86.1 and 88.5% of the radioactivity inthe NPs at t = 48 h for DOTA-2000-MNPs and DOTA-t-PApep.1$_{LAC}$- 2000-MNPs, respectively. DOTA-t-PApep.1$_{LAC}$-2000-MNPs showed a higher stability in the presence of a competitor, with around 50% of the radioactivity still attached to the MNP after 24 h. A lower stability of the label was found for DOTA-2000-MNPs, where more than 70% of the ^{67}Ga was released from the MNPs after 24 h (SI, Table S5).

3.5. SPECT–CT imaging

Five mice per sample were subjected to longitudinal SPECT–CT acquisitions at 3, 24, and 48 h after administration of the ^{67}Ga-MNPs.DOTA-2000-MNPs and DOTA-t-PApep.1$_{LAC}$-2000-MNP were mainlyaccumulated into the liver (see Fig. 4). The analysis of tumour/muscleratios for both MNPs presented similar values at all time-points (SI, Figure S5). A significant increase from 3 h to 24 h and from 3 h to48 h was observed for both MNPs.

3.6. Handheld gamma camera

Images also were acquired using a handheld gamma camera withthe aim of comparing the results obtained with the other imaging methods. After injection of ^{67}Ga-labelled NPs, mice were positioned on the on top of the handheld gamma camera using the specimen platform. Image acquisition was performed using an energy window of 80keV–105 keV. For all acquisitions the handheld gamma camera was equipped using the LEHR collimator. During the whole acquisition, theanimals were under isoflurane anaesthesia (1.5%–2% in oxygen). Acquisitions were performed 3 h and 24 h after injection, just after finishing the SPECT acquisitions (SI, Figure S6). Data were d using a self-developed software toolkit. ROI analysis was used to calculate the mean counts measured in the tumour, the liver, and the background.

In case of DOTA-2000-MNP, tumour-to-liver ratios are very low,demonstrating the massive accumulation of the NPs in the liver. Highertumour-to-background ratios were obtained over time (SI, Tables S6and S7). Looking at these ratios, there was a non-significant increaseof uptake in the tumour over time, that was more evident for the targeted versus the non-targeted particles, but it has to be kept in mind that the background signal was high in both cases.

4. Discussion

In the present preclinical study, MNPs with and without an attachedtargeting moiety for pancreatic cancer were tested with respect to theircapabilities for in vivo medical imaging using MRI, SPECT–CT, and a handheld gamma camera. Increased relaxation rates

in MRI or increased radiation ratios for tumour/muscle in SPECT–CT and handheld gamma camera imaging were found for targeted as well as for non-targeted MNPs evidencing their uptake by the tumours. This uptake can be explained by passive accumulation of particles via leaky endothelia in tumours combined with the tumours' poor lymphatic drainage. As shown in previous investigations, no difference in in vitro and in vivo toxicityand behaviour of MNPs containing different amounts of iron in formof CAN maghemite [15] was observable compared to untreated controls.Because of its relevance for the clinics, the results obtained with the 1.5 T MRI human scanner are of special interest. This technique directly visualizes the particles' uptake without having to depend on the in vivobinding stability of the attached radiolabels required for SPECT-CT or handheld gamma camera.

By evaluating only the 1.5 T MRI's SI of the different tissues, no significant uptake of 4000-MNPs, neither non-targeted nor targeted, was detectable (see SI Table S3). However, by additionally analysing the spin– spin–relaxation rate (R2) a significantly higher uptake of targeted 4000- MNPs compared to non-targeted 4000-MNPs in the sc tumour (Fig. 3,C1, C2, D1, and D2) was detectable. R2 in general is superior to conventional SI evaluation in terms of quantification of low iron concentrations, because it evaluates not only a single point in time butquantifies the relaxation process itself. The difference between the targeted 4000-MNP and non-targeted 4000-MNPs was significant after calculating the R2–Spin–Spin–relaxation rates according to a protocol by Weis et al. [24]. The maghemite-based nanoparticles shownin this publication, are super-paramagnetic contrast agents, and, therefore, influence the T2 contrast of a tissue in terms of a signal intensity decrease caused by an increase of relaxation rates in the presence ofthese NPs. This accumulation can be recorded dynamically with subsequent T2w images and furthermore quantified by T2 relaxation mapping.

The MRI's R2-rate for targeted 4000-MNP and non-targeted 4000- MNP (SI Table S4) was increased after MNP administration. Moreover,the sc tumour's R2-rate was 1.76-fold higher in case of the targeted NP compared to the non-targeted ones. This increased uptake was a result attributed to the targeting moiety t-PApep.1$_{LAC}$ [17], which, after acovalent linkage to 4000-MNPs, results in a higher uptake rate of these NPs into pancreatic cancer cells as seen in previous in vitro experiments.

Analysis of the results of SPECT–CT and the handheld gamma camera showed no differences between non-targeted and targeted DOTA-2000-MNPs. Both particles have significantly increased tumour/muscle ratio from 3 h to 48 h and thus slowly accumulated in the pancreatic tumour.Similar time-courses were obtained by the handheld gamma camera.These findings are in agreement with the results obtained for both DOTA-2000-MNPs at 11.7 T, which displayed no signal alteration withinthe first 90 min following particle administration, however qualitative signal changes were detectable after 24 h. Thus, the use of SPECT/CT (Ga[67] half-life 3.26 days) over PET/CT (Ga[68] half-life 68 min) in combination with longitudinal MRI might be ideally suited to assess biodistribution and kinetics of slowly equilibrating nanoparticles (days) in vivo.

Furthermore, the in vivo tests performed in the present study alsodemonstrated the absence of histological and behavioural changes in-dicative of toxicity problems (SI, *Histology and behavioural toxicology tests,* SI Table S8, SI Figure S7). The latter results were expected since HSA nanoparticles already previously were well tolerated, as shownby an earlier study [15] as well as by clinical experiences with registeredHSA particle-based formulations such as Albunex™ and Abraxane™ [25].

5.Conclusions

The present study demonstrated that all imaging modalities - MRI, SPECT-CT, and handheld gamma camera – were able to

detect an in vivo accumulation of human serum albumin nanoparticles over time in PANC1-tumours, a tumour-model for adenocarcinoma of thepancreas. Although nanoparticles – like other colloids including liposomes or many macromolecules in general – were taken up by the reticuloendothelial system (RES), especially the liver to a high percentage(up to 90% of the administered dose), a significant amount of the remaining fraction of circulating nanoparticles was shown to accumulate in pancreatic tumour tissue by all imaging modalities. Whereas conventional MRI, SPECT–CT, and handheld gamma camera were not able to distinguish between targeted and non-targeted nanoparticles, MRI-based R2 relaxometry at 1.5 T was able to detect an increased uptakefor the t-PApep.1$_{LAC}$-targeted vs. the non-targeted nanoparticles.

This result provides a platform for the fine-tuning of the diagnostic possibilities of non-toxic human serum albumin nanoparticles especially in hypoperfused adenocarcinomas of the pancreas and, further down the road, for the development of theranostics for these types of cancer.

Appendix A. Supplementary data

Supplementary data to this article can be found online at http://dx.doi.org/10.1016/j.jconrel.2015.07.017.

References

[1] American-Cancer-Society, Cancer Facts & Figs. 2014, in: A.C. Society (Ed.) AmericanCancer Society, Atlanta, 2014.

[2] L. Rahib, B.D. Smith, R. Aizenberg, A.B. Rosenzweig, J.M. Fleshman, L.M. Matrisian,Projecting cancer incidence and deaths to 2030: the unexpected burden of thyroid, liver, and pancreas cancers in the United States, Cancer Res. 74 (2014) 2913-2921.

[3] Robert-Koch-Institut, G.d.e.K.i.D.e. V., Krebs in Deutschland 2009/2010, 2013. (in,Berlin).

[4] T. Muniraj, P.A. Jamidar, H.R. Aslanian, Pancreatic cancer: a comprehensive reviewand update, Dis. Mon. 59 (2013) 368–402.

[5] NCI, SEER Stat Fact Sheets: Pancreas Cancer, in: N.C. Institute (Ed.), 2014.

[6] A. Stathis, M.J. Moore, Advanced pancreatic carcinoma: current treatment and futurechallenges, Nat. Rev. Clin. Oncol. 7 (2010) 163–172.

[7] T.M. van Gulik, T.M. Moojen, R. van Geenen, E.A. Rauws, H. Obertop, D.J. Gouma, Differential diagnosis of focal pancreatitis and pancreatic cancer, Ann. Oncol. 10 (Suppl. 4) (1999) 85–88.

[8] K. Sandrasegaran, K. Nutakki, B. Tahir, A. Dhanabal, M. Tann, G.A. Cote, Use of diffusion-weighted MRI to differentiate chronic pancreatitis from pancreatic cancer, AJR Am. J. Roentgenol. 201 (2013) 1002–1008.

[9] S. Dreis, F. Rothweiler, M. Michaelis, J. Cinatl Jr., J. Kreuter, K. Langer, Preparation,characterisation and maintenance of drug efficacy of doxorubicin-loaded humanserum albumin (HSA) nanoparticles, Int. J. Pharm. 341 (2007) 207–214.

[10] S. Wohlfart, A.S. Khalansky, C. Bernreuther, M. Michaelis, J. Cinatl Jr., M. Glatzel, J.Kreuter, Treatment of glioblastoma with poly(isohexyl cyanoacrylate) nanoparticles,Int. J. Pharm. 415 (2011) 244-251.

400 [11] H. Wartlick, K. Michaelis, S. Balthasar, K. Strebhardt, J. Kreuter, K. Langer, Highly spe-cific HER2-mediated cellular uptake of antibody-modified nanoparticles in
401 tumour cells, J. Drug Target. 12 (2004) 461–471.

402 [12] H. Maeda, J. Wu, T. Sawa, Y. Matsumura, K. Hori, Tumor vascular permeability andthe EPR effect in macromolecular therapeutics: a review, J. Control. Release
403 65 (2000) 271–284.

404 [13] K. Ulbrich, T. Hekmatara, E. Herbert, J. Kreuter, Transferrin- and transferrin- receptor-antibody-modified nanoparticles enable drug delivery across the
405 blood- brain barrier (BBB), Eur. J. Pharm. Biopharm. 71 (2009) 251–256.

406 [14]

407   A. Zensi, D. Begley, C. Pontikis, C. Legros, L. Mihoreanu, C. Buchel, J. Kreuter, Humanserum albumin nanoparticles modified with apolipoprotein A-I cross the
408   blood- brain barrier and enter the rodent brain, J. Drug Target. 18 (2010) 842–848.

409   [15] I. Rosenberger, C. Schmithals, J. Vandooren, S. Bianchessi, P. Milani, E. Locatelli, L.L.Israel, F. Hübner, M. Matteoli, J.-P. Lellouche, M.C. Franchini, L. Passoni, E.
410   Scanziani,

411   G. Opdenakker, A. Piiper, J. Kreuter, Physico-chemical and toxicological characteriza-tion of iron-containing albumin nanoparticles as platforms for medical imaging,
412   J.Control. Release 194 (2014) 130–137.

413   [16] H. Korkusuz, K. Ulbrich, K. Welzel, V. Koeberle, W. Watcharin, U. Bahr, V. Chernikov,

414   T. Knobloch, S. Petersen, F. Huebner, H. Ackermann, S. Gelperina, W. Kromen, R. Hammerstingl, J. Haupenthal, F. Gruenwald, J. Fiehler, S. Zeuzem, J. Kreuter,
415   T.J. Vogl, A. Piiper, Transferrin-coated gadolinium nanoparticles as MRI contrast agent, Mol. Imaging Biol. 15 (2013) 148–154.

416   [17] O. Roda, E. Ortiz-Zapater, N. Martinez-Bosch, R. Gutierrez-Gallego, M. Vila-Perello, C.Ampurdanes, H.J. Gabius, S. Andre, D. Andreu, F.X. Real, P. Navarro,
417   Galectin-1 is anovel functional receptor for tissue plasminogen activator in pancreatic cancer, Gas- troenterology 136 (2009) 1379–1390 (e1371–1375).

418   [18] S. Pan, R. Chen, B.A. Reimel, D.A. Crispin, H. Mirzaei, K. Cooke, J.F. Coleman, Z. Lane,

419   M.P. Bronner, D.R. Goodlett, M.W. McIntosh, W. Traverso, R. Aebersold, T.A. Brentnall, Quantitative proteomics investigation of pancreatic intraepithelial
420   neoplasia, Electrophoresis 30 (2009) 1132–1144.

421   [19] J. Shen, M.D. Person, J. Zhu, J.L. Abbruzzese, D. Li, Protein expression profiles inpancreatic adenocarcinoma compared with normal pancreatic tissue and
422   tissue af-fected by pancreatitis as detected by two-dimensional gel electrophoresis and massspectrometry, Cancer Res. 64 (2004) 9018–9026.

423   [20] L. Nobs, F. Buchegger, R. Gurny, E. Allemann, Poly(lactic acid) nanoparticles labeledwith biologically active Neutravidin for active targeting, Eur. J. Pharm.
424   Biopharm. 58(2004) 483–490.

425   [21] E.A. Fragogeorgi, I.N. Savina, T. Tsotakos, E. Efthimiadou, S. Xanthopoulos, L. Palamaris, D. Psimadas, P. Bouziotis, G. Kordas, S. Mikhalovsky, M. Alavijeh,
426   G. Loudos, Comparative in vitro stability and scintigraphic imaging for trafficking and tumor targeting of a directly and a novel 99mTc(I)(CO)3 labeled
427   liposome,Int. J. Pharm. 465 (2014) 333–346.

428   [22] L. Stelter, J.G. Pinkernelle, R. Michel, R. Schwartlander, N. Raschzok, M.H. Morgul, M.Koch, T. Denecke, J. Ruf, H. Baumler, A. Jordan, B. Hamm, I.M. Sauer, U.
429   Teichgraber, Modification of aminosilanized superparamagnetic nanoparticles: feasibility of multimodal detection using 3 T MRI, small animal PET, and
430   fluorescence imaging, Mol. Imaging Biol. 12 (2010) 25–34.

431   [23] P. Knoll, S. Mirzaei, K. Schwenkenbecher, T. Barthel, Performance evaluation of asolid-state detector based handheld gamma camera system, Front. Biomed.
432   Technol.1 (2014) 61–67.

433   [24] C. Weis, F. Blank, A. West, G. Black, R.C. Woodward, M.R. Carroll, A. Mainka, R. Kartmann, A. Brandl, H. Bruns, E. Hallam, J. Shaw, J. Murphy, W.Y. Teoh,
434   K.E. Aifantis, R. Amal, M. House, T.S. Pierre, B. Fabry, Labeling of cancer cells with mag-netic nanoparticles for magnetic resonance imaging, Magn. Reson. Med.
435   71 (2014) 1896-1905.

436   [25] A.O. Elzoghby, W.M. Samy, N.A. Elgindy, Albumin-based nanoparticles as potential controlled release drug delivery systems, J. Control. Release 157 (2012)
437   168–182.

438
439
440
441
442
443
444
445
446
447
448
449
450
451
452

453 Tables

Table 1
Amount of attached t-PApep.1LAC per 5 mg MNP and per MNP.

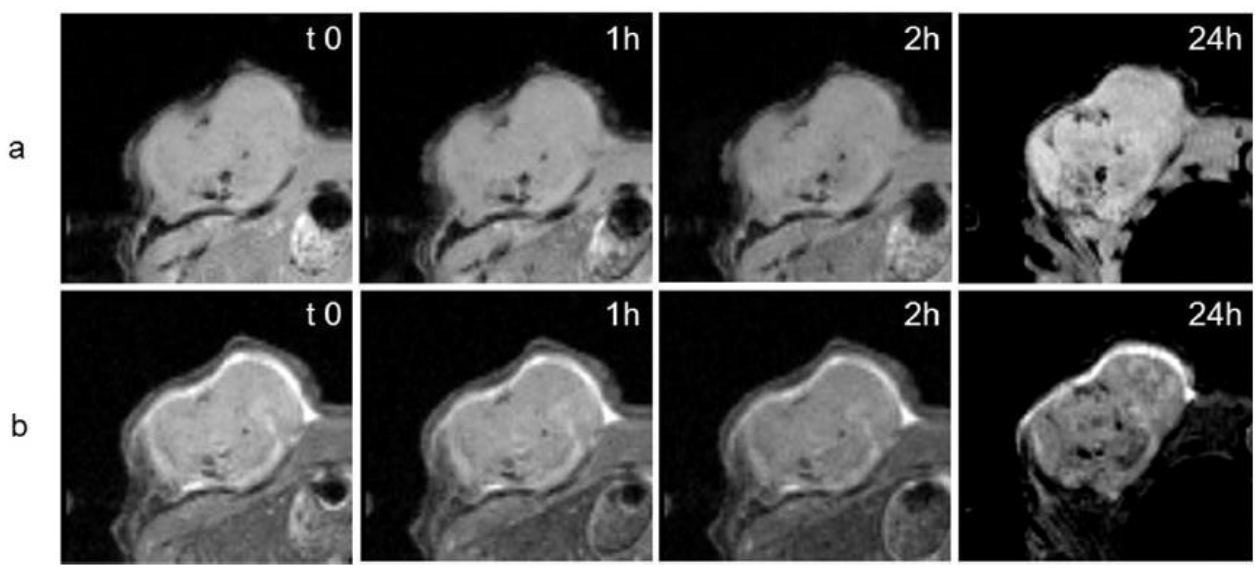|	Attached t-PApep.1$_{LAC}$ [μg/5 mg MNP]	t-PApep.1$_{LAC}$/MNP
DOTA-2000-MNP	37.81 ± 0.13	2726 ± 9
4000-MNP	45.63 ± 0.17	8321 ± 31

454

Table 2
R2 before (pre) and after (post) NP administration, normalized to the muscle value.

sc Tumour	R2 pre (in 1/s), normalized to muscle	R2 post (in 1/s), normalized to muscle
4000-MNP	0.13 ± 0.12	0.25 ± 0.05
t-PApep.1$_{LAC}$-4000-MNP	0.16 ± 0.09	0.44 ± 0.11

455
456 Figures

457
458 Fig. 1. Representative zoomed T1-weighted (a) and T2-weighted (b) images of a single slice showing the temporal evolution of DOTA-tPapep.1$_{LAC}$-2000-MNP.MNPs were

459 injected after t0 within the scanner. The 24 h time-points were acquired after animal reposition.
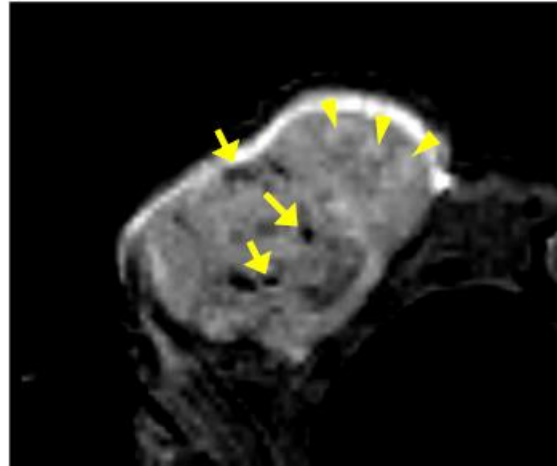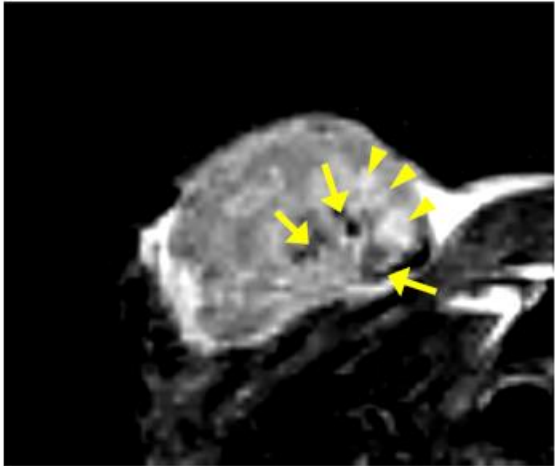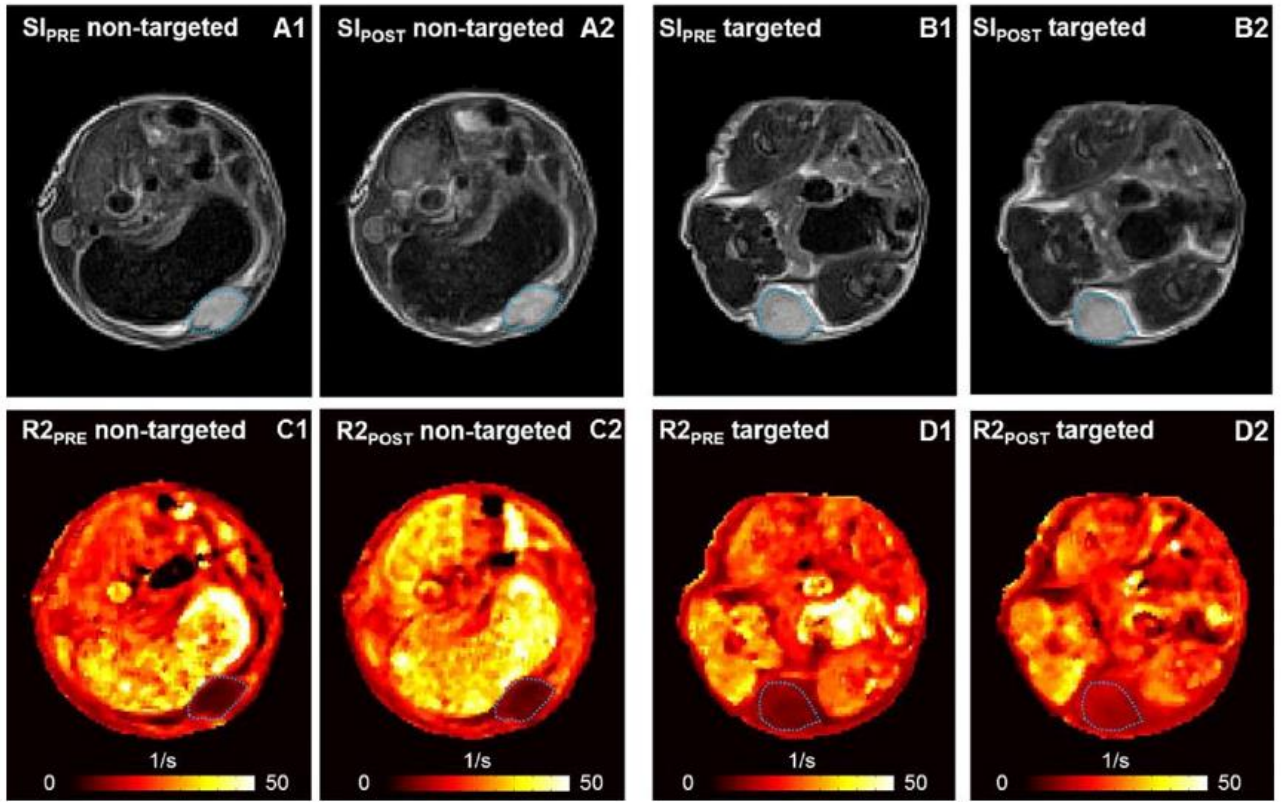
460
461
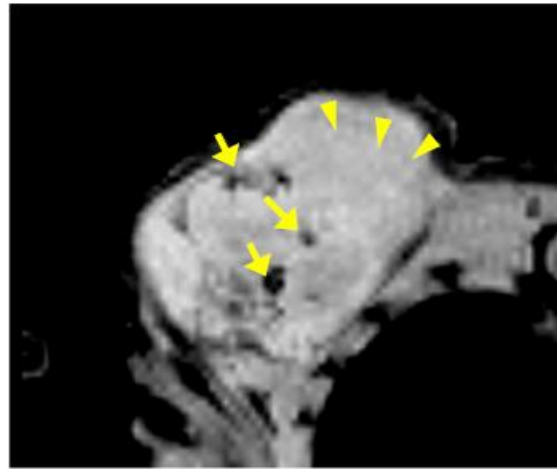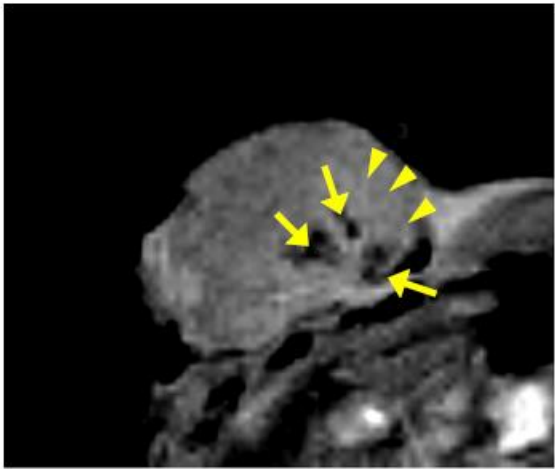
Fig. 2. Representative zoomed T1-weighted (a) and T2-weighted (b) images of a single slice 24 h after MNPs injection. Arrows show representative zones for dark focal spots whereas arrowheads indicate diffuse bright regions

462
463
464

Fig. 3. Representative slices ofmouseMRI-datasets before and 90 min afterMNP administration. A1, A2, B1, and B2 showconventional signal intensity. C1, C2, D1, and D2 showspin–spin–relaxation rate (R2). The images on the left (A1, A2, C1, and C2) were acquired before and after an injection of non-targeted nanoparticles, the images on the right (B1, B2, D1, and D2) were acquired before and after an injection of targeted nanoparticles. The sc tumours' outer boundaries are indicated in light blue.Whereas there was no significant difference between the signal intensities of the sc tumours after administration of non-targeted and targeted nanoparticles, the sc tumour expressed a significantly higher R2 in case of the injection of targeted nanoparticles (0.44 ± 0.11 1/s, normalized to muscle) compared to the non-targeted nanoparticle injection (0.25 ± 0.05 1/s, normalized to muscle).

484
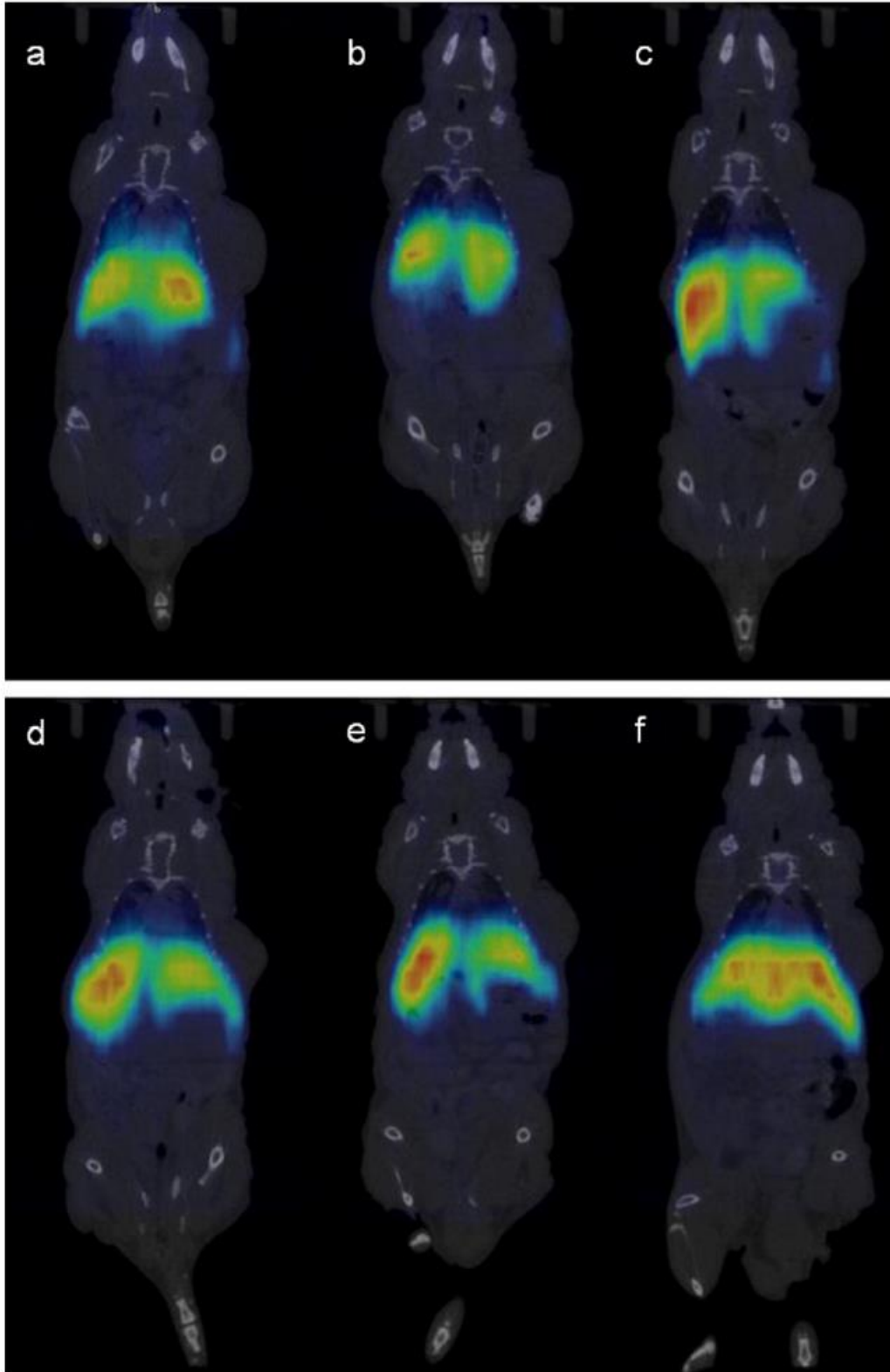
485　Fig. 4. SPECT–CT images of the biodistribution of 67Ga-DOTA-2000-MNPs (a–c) and 67Ga-DOTA-t-PApep.1LAC-2000-MNP (d–f) at t=3 h (a,d), 24 h (b,e), and 48 h (c,f) after

486　intravenous administration. Doses: 6.5 ± 0.4 MBq for DOTA-2000-MNP, 6.6 ± 1.3 MBq for DOTA-t-PA-2000-MNPs, V = 150–200 µL in physiologic saline.